

## A Time-Splitting Scheme for the Elastic Equations Incorporating Second-Order Runge–Kutta Time Differencing

LOUIS J. WICKER

*Department of Meteorology, Texas A&M University, College Station, Texas*

WILLIAM C. SKAMAROCK

*National Center for Atmospheric Research,\* Boulder, Colorado*

(Manuscript received 7 April 1997, in final form 23 October 1997)

### ABSTRACT

A forward-in-time splitting method for integrating the elastic equations is presented. A second-order Runge–Kutta time integrator (RK2) for the large-time-step integration is combined with the forward–backward scheme in a manner similar to the Klemp and Wilhelmson method. The new scheme produces fully second-order-accurate integrations for advection and gravity wave propagation. The RK2 scheme uses upwind discretizations for the advection terms and is easily combined with standard vertically semi-implicit techniques so as to improve computational efficiency when the grid aspect ratio becomes large. A stability analysis of the RK2 split-explicit scheme shows that it is stable for a wide range of advective and acoustic wave Courant numbers.

The RK2 time-split scheme is used in a full-physics nonhydrostatic compressible cloud model. The implicit damping properties associated with the RK2's third-order horizontal differencing allows for a significant reduction in the value of horizontal filtering applied to the momentum and pressure fields, while qualitatively the solutions appear to be better resolved than solutions from a leapfrog model.

### 1. Introduction

In atmospheric models integrating the hydrostatic or nonhydrostatic equations, physical modes of meteorological importance are often of much lower frequency than the highest-frequency modes admitted by the equations. For the hydrostatic system the high-frequency mode is the external mode (the Lamb wave), while for the nonhydrostatic system the high-frequency modes are the acoustic waves. In numerical models, the time step needed to stably integrate the high-frequency modes are often 2–10 times smaller than the time step needed for stable and accurate integration of the low-frequency modes. A common strategy for improving computational efficiency is to employ explicit numerical schemes that integrate the high-frequency modes using a small time step while integrating the lower-frequency modes using a larger, and therefore more economical, time step. These methods are often called splitting methods (Marchuk 1974), and several different splitting

methodologies based on explicit integration schemes exist.

One of the most commonly used splitting methods for the compressible nonhydrostatic equations was introduced by Klemp and Wilhelmson (1978, hereafter KW), and it employs a leapfrog time discretization for the terms associated with the low-frequency modes and a forward–backward scheme (Mesinger 1977) for the terms responsible for the propagation of the high-frequency acoustic modes. Skamarock and Klemp (1992, hereafter SK92) analyzed the stability of the KW scheme as well as other potential split-explicit schemes. They found that the KW scheme possessed the best combination of stability, simplicity, and minimal filtering of the schemes they considered.

SK92 also analyzed explicit time-splitting schemes, based on the KW methodology, that used forward-in-time methods for the slow modes and the forward–backward scheme for the fast modes. They found that the schemes had significant instabilities and that even with filtering, these splitting methods were not suitable for explicit time-split models. However, forward-in-time methods, such as Smolarkiewicz (1984) and Tremback et al. (1987), represent viable approximations for the advection terms in the momentum equations if suitable time-splitting approaches can be found. These forward-in-time schemes are often formulated using upwind and/or monotonic techniques that reduce phase errors and

---

\* The National Center for Atmospheric Research is sponsored by the National Science Foundation.

---

*Corresponding author address:* Dr. Louis J. Wicker, 1204 Eller O&M Bldg., College Station, TX 77843-3150.  
E-mail: wicker@ariel.met.tamu.edu

reduce or eliminate the presence of spurious oscillations generated from underresolved gradients. The pure forward schemes have the attractive advantage that the number of small steps needed to integrate the high-frequency modes would potentially be half that needed for the KW scheme when used with the forward-backward scheme of Mesinger because the fast modes are integrated from  $t$  to  $t + \Delta t$  as opposed to  $t - \Delta t$  to  $t + \Delta t$ . Therefore, combining forward-in-time schemes for the advective terms with the forward-backward method for the high-frequency modes would present an attractive alternative to KW.

In this paper we describe a forward-in-time split-explicit scheme that is a viable alternative to the KW scheme for the integration of the nonhydrostatic compressible equations. A second-order Runge-Kutta method is used as the time integration scheme for the advective terms and the forward-backward scheme is used for the acoustic terms. The Runge-Kutta method retains the advantages associated with many forward schemes; for example, it uses upwind discretizations for the spatial differences and can be formulated as a monotonic method (Hundsdoerfer et al. 1995), although it requires three-quarters the number of the small time steps compared with KW. Tests using this new scheme in both two- and three-dimensional nonhydrostatic models show the scheme is stable and accurate.

## 2. Scheme formulation and stability

The formulation and stability of the scheme can be considered using a simplified one-dimensional set of equations that describe the propagation and advection of acoustic waves:

$$\frac{\partial u}{\partial t} + \frac{\partial \pi}{\partial x} = -u \frac{\partial u}{\partial x}. \quad (1)$$

$$\frac{\partial \pi}{\partial t} + c_s^2 \frac{\partial u}{\partial x} = -u \frac{\partial \pi}{\partial x}. \quad (2)$$

Equations (1) and (2) are the horizontal momentum and pressure equations, respectively, where  $u$  is the fluid velocity in the  $x$  direction,  $\pi$  is the perturbation Exner pressure,  $t$  is time, and  $c_s$  is the sound speed. A linear version of the system (1) and (2) is equivalent to the system used by SK92 to analyze the basic properties of various time-splitting schemes. We will concern ourselves with discretizations on the C grid. Although the computation of advection terms is more expensive on the C grid than on a nonstaggered grid, the C grid has the advantage of accurately resolving the gravity wave modes (Haltiner and Williams 1980, 227).

### a. Formulation

We wish to retain, in the Runge-Kutta-based scheme, the core methodology associated with the KW scheme, that is, to evaluate the terms responsible for advection

using a single large time step while integrating the terms responsible for the acoustic problems using a smaller time step. We choose a second-order Runge-Kutta method [Press et al. (1986), 550; hereafter RK2] as the large-time-step scheme used to integrate the dependent variables in (1) and (2) from  $t$  to  $t + \Delta t$ . There are several formulations for second-order Runge-Kutta methods; the RK2 scheme used here is sometimes referred to as the ‘‘improved polygon’’ method and can be written as

$$\phi^* = \phi^t + \frac{\Delta t}{2} \mathbf{F}(\phi^t), \quad (3a)$$

$$\phi^{t+\Delta t} = \phi^t + \Delta t \mathbf{F}(\phi^*), \quad (3b)$$

where  $\mathbf{F}$  is a forcing vector of the dependent variables, the superscripts indicate the time level, and the forcing can be a function of all the relevant dependent variables. The RK2 scheme is absolutely unstable for the pure oscillation equation,  $\phi_t = i\omega\phi$ . Pure linear advection can be represented by the oscillation equation where  $\omega$  is replaced by  $kU$  ( $k$  is the wavenumber  $2\pi/L$ ). Thus for pure advection, the RK2 method is only stable when combined with spatial discretizations that are upwind biased, that is, the leading truncation error term is even ordered and dissipative. Thus the effective frequency in the discrete system possesses complex frequencies with negative real parts that, taken together with the imaginary parts, produce a stable scheme. Conversely, the RK2 scheme is unstable when the spatial derivatives are centered because the real part of the discrete frequency is 0. While any upwind discretization can be used, we have found the third-order upwind spatial discretization to be a good compromise between efficiency and accuracy. For positive flow ( $u > 0$ ), the third-order RK2 scheme can be written as

$$\phi^* = \phi^t - \frac{u\Delta t}{12\Delta x} R(\phi^t), \quad (4a)$$

$$\phi^{t+\Delta t} = \phi^t - \frac{u\Delta t}{6\Delta x} R(\phi^*), \text{ and} \quad (4b)$$

$$R(\phi) = \phi_{i-2} - 6\phi_{i-1} + 3\phi_i + 2\phi_{i+1}. \quad (4c)$$

A more general version of the  $R$  operator for both positive and negative flows, which requires no special switches for the upwind direction, can be found in Hundsdoerfer et al. (1995). Figure 1 shows the amplification factor for the third-order RK2 scheme for the case of pure advection. This scheme is stable for all wavenumbers when the advective Courant number is less than 0.88. As expected from the Taylor series analysis, the scheme heavily damps wavenumbers greater than  $\pi/2$  (wavelengths less than  $4\Delta x$ ). Linear advection tests (not shown) indicate that the scheme has small phase errors and that the scheme’s inherent numerical damping helps control oscillations generated from underresolved gradients in the advected quantity. We find

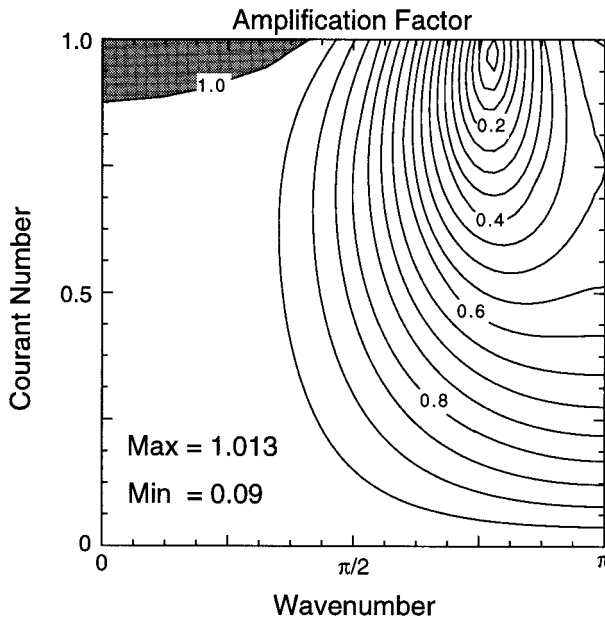


FIG. 1. Amplification factor for RK2 scheme with third-order spatial discretization. Contour interval is 0.05. Maximum and minimum values are plotted at the lower left. The shaded region indicates where the scheme is unstable.

that the third-order scheme performs satisfactorily in our full Navier–Stokes models.

Similar to KW, a forward–backward time scheme with centered spatial derivatives is used to integrate the pressure gradient and divergence terms in (1) and (2). We divide the new scheme into two major steps. First, the large time step tendencies are defined using the third-order spatial differencing,

$$f_u^t = -\frac{u_i^t}{6\Delta x}R(u^t) \quad \text{and} \quad (5a)$$

$$f_\pi^t = -\frac{\overline{u_i^t}}{6\Delta x}R(\pi^t), \quad (5b)$$

where  $\overline{\phi^x} = \frac{1}{2}(\phi_{x+\Delta x/2} + \phi_{x-\Delta x/2})$ . The middle-time-level predictors are produced by integrating the slow and fast modes forward, to the midpoint of the time step ( $\Delta t/2$ ), using a small time step with the slow-mode tendencies (5a) and (5b) held fixed. The fast-mode scheme is the forward–backward scheme of Mesinger (1977), and the small-time-step equations are

$$u_i^{\tau+\Delta\tau} = u_i^\tau - \frac{\Delta\tau}{\Delta x}\delta_x\pi^\tau + \Delta\tau f_u^t \quad \text{and} \quad (5c)$$

$$\pi_i^{\tau+\Delta\tau} = \pi_i^\tau - \frac{c_s^2\Delta\tau}{\Delta x}\delta_x u^{\tau+\Delta\tau} + \Delta\tau f_\pi^t, \quad (5d)$$

where  $\delta_x\phi = (1/\Delta x)(\phi_{x+\Delta x/2} - \phi_{x-\Delta x/2})$ . Here the small time step  $\Delta\tau = \Delta t/n_s$ , and  $n_s/2$  small time steps<sup>1</sup> are

<sup>1</sup> Note that for the RK2 time-split scheme,  $n_s$  must be an even number.

used to advance to the midpoint of the large time step. To complete the large time step, the advective tendencies are now recomputed using the predicted midpoint values

$$f_u^{t+\Delta t/2} = -\frac{u_i^{t+\Delta t/2}}{6\Delta x}R(u^{t+\Delta t/2}) \quad \text{and} \quad (5e)$$

$$f_\pi^{t+\Delta t/2} = -\frac{u^{t+\Delta t/2}}{6\Delta x}R(\pi^{t+\Delta t/2}), \quad (5f)$$

and the small step integration is then repeated starting with the values at the original time level  $t$  and advanced to  $t + \Delta t$  using

$$u_i^{\tau+\Delta\tau} = u_i^\tau - \frac{\Delta\tau}{\Delta x}\delta_x\pi^\tau + \Delta\tau f_u^{t+\Delta t/2} \quad \text{and} \quad (5g)$$

$$\pi_i^{\tau+\Delta\tau} = \pi_i^\tau - \frac{c_s^2\Delta\tau}{\Delta x}\delta_x u^{\tau+\Delta\tau} + \Delta\tau f_\pi^{t+\Delta t/2}, \quad (5h)$$

through  $n_s$  small time steps. The complete RK2 time-split scheme is described by (5a) through (5h).

### b. Stability analysis

Using the methodology presented in the appendix of SK92, a stability analysis was performed on scheme (5). For this analysis, a linearized version of (1) and (2) is used:

$$\frac{\partial u}{\partial t} + c_s \frac{\partial \pi}{\partial x} = -U \frac{\partial u}{\partial x} \quad \text{and} \quad (6a)$$

$$\frac{\partial \pi}{\partial t} + c_s \frac{\partial u}{\partial x} = -U \frac{\partial \pi}{\partial x}, \quad (6b)$$

where  $U$  is the mean advective velocity,  $c_s$  is a constant sound speed, and for convenience we have redefined  $\pi$  to be  $\pi/c_s$ . The analysis examines a spatial Fourier decomposition of the discretization (5). For example, the small-time-step counterparts to (5c) and (5d) lead to

$$u^{\tau+\Delta\tau} = u^\tau - i\lambda_{cx}\pi^\tau - \frac{i}{n_s}\lambda_u u^\tau \quad \text{and} \quad (7a)$$

$$\pi^{\tau+\Delta\tau} = \pi^\tau - i\lambda_{cx}u^{\tau+\Delta\tau} - \frac{i}{n_s}\lambda_u\pi^\tau, \quad (7b)$$

where

$$\lambda_{cx} = \frac{2c_s\Delta\tau}{\Delta x} \sin\left(\frac{k\Delta x}{2}\right) \quad \text{and}$$

$$\lambda_u = \frac{U\Delta t}{\Delta x} \frac{1}{6} \left\{ i \left[ \cos\left(\frac{4\pi\Delta x}{L}\right) - 4 \cos\left(\frac{2\pi\Delta x}{L}\right) \right] + \left[ \sin\left(\frac{4\pi\Delta x}{L}\right) - 8 \sin\left(\frac{2\pi\Delta x}{L}\right) \right] \right\},$$

where  $k = 2\pi/L$  is a horizontal wavenumber. Using this formalism, the amplification matrix is constructed as in SK92 and its eigenvalues are computed numerically.

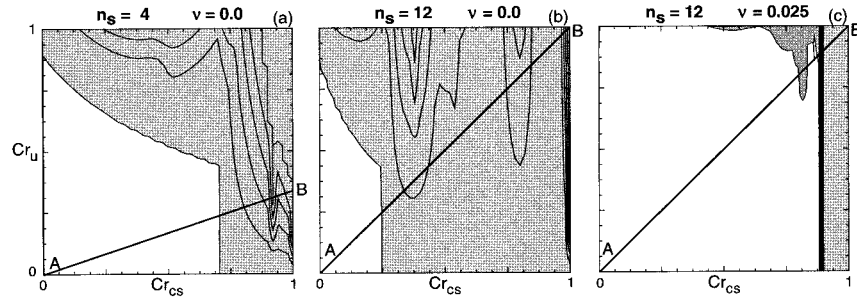


FIG. 2. Maximum amplification factor for the split-explicit third-order RK2 scheme. The contour interval is 0.1 and  $Cr_u$  and  $Cr_{cs}$  are the advective and sound speed Courant numbers, respectively; (a)  $n_s = 4$ , (b)  $n_s = 12$ , (c)  $n_s = 12$ , with a divergence damping coefficient  $\alpha = 0.025$ . The lines  $AB$  are plotted using  $U/c_s = 1/12$ , and shaded regions indicate where the amplification factor is greater than 1.

The results of this stability analysis are presented in Fig. 2 where the maximum absolute value of the eigenvalues is contoured as a function of advective ( $U\Delta t/\Delta x$ ) and acoustic ( $c_s\Delta\tau/\Delta x$ ) Courant numbers from (7a) and (7b) for the case of  $n_s = 4$  and  $n_s = 12$ . Schemes are stable when the absolute value of the eigenvalues are less than or equal to 1, and here the maximum absolute eigenvalue is for spatial wavelengths  $2\Delta x$  through  $20\Delta x$ . With four small time steps per large time step (Fig. 2a), there exists a large region where the amplification matrix is less than or equal to 1. The stability region of interest is below and to the right of the thick lines in Fig. 2, where the slope of the line is the  $U\Delta t/c_s\Delta\tau$ .<sup>2</sup> As the number of small time steps are increased to 12 (Fig. 2b) there are regions of instability entering the lower right-hand portion of the domain that are troublesome. SK92 showed that the unfiltered KW scheme also has similar instabilities and that the Asselin time filter stabilizes the scheme. SK92 introduced a divergence damping filter that also stabilizes the KW scheme. Divergence damping has the advantage that it only damps acoustic modes and not the nondivergent modes, and preserves the second-order temporal accuracy of the scheme. Including a divergence damping filter in the RK2 scheme also significantly reduces the instabilities. Divergence damping takes the form of a second-order dissipation term for the pure 1D acoustic system (6), and its inclusion results in replacing (6a) by

$$\frac{\partial u}{\partial t} + c_s \frac{\partial \pi}{\partial x} = -U \frac{\partial u}{\partial x} + \nu \frac{\partial D}{\partial x}, \quad (8)$$

where  $D$  is the velocity divergence (here  $D = \delta_x u$ ). Stability results with divergence damping included are given in Fig. 2c for the case  $n_s = 12$  and a nondimen-

sional divergence damping coefficient  $\alpha = 0.025$  ( $\alpha = \nu\Delta\tau/\Delta x^2$ ). Stability is recovered in most of the parameter space.

### 3. Numerical tests

#### a. Propagating gravity wave simulations

Skamarock and Klemp (1994, hereafter SK94) analyzed the efficiency and accuracy of the KW scheme by simulating the propagation of inertia-gravity waves on both nonhydrostatic and hydrostatic scales. Analytical solutions for their examples are given in SK94 and here we compare solutions for the RK2 and KW schemes with the analytical solutions in both regimes.

The test problem simulates the propagation of an inertia-gravity wave in a Boussinesq atmosphere of constant Brunt-Väisälä frequency with  $N = 10^{-2} \text{ s}^{-1}$ , in a periodic channel with solid, free-slip upper and lower boundaries, with a mean wind  $U = 20 \text{ m s}^{-1}$  translating the waves. In the small time step of the RK2 and leapfrog models,  $w$ ,  $\pi$ , and  $\theta$  are advanced using the vertically implicit scheme described in SK92, which is time centered [ $\beta = 0$  in SK92 Eqs. (28) and (29)], thus removing any vertically propagating acoustic wave or buoyancy-oscillation time step restrictions. The horizontal advection terms for the RK2 scheme are computed using the third-order upwind spatial discretization. For vertical advection, second-order centered finite differences are combined with the RK2 time differencing. This vertical discretization was chosen for simplicity. Formally maintaining third-order accuracy in  $z$  is complicated; however, third-order differencing in computational space could be used, resulting in third-order accuracy in the transformed coordinate. We discretize the Coriolis terms in the simple model using a forward-in-time approach, which is also formally unstable. However, linear stability analysis shows that for the size of the time steps used below, the amplification rate is so small that instabilities would require more than  $10^4$  time steps before significant growth in the solution would be observed. Simulations requiring long-

<sup>2</sup> The advective velocities in a simulation can vary up to  $U_{\max}$ , while the sound speed  $c_s$  is fixed. So while in the linear case with fixed  $U$  and  $c_s$  we are technically interested only in the stability along the thick lines in Fig. 2, in practice the schemes must be stable below these lines because  $U < U_{\max}$ . If  $c_s$  were similarly variable, we would need to examine the stability across the entire space.

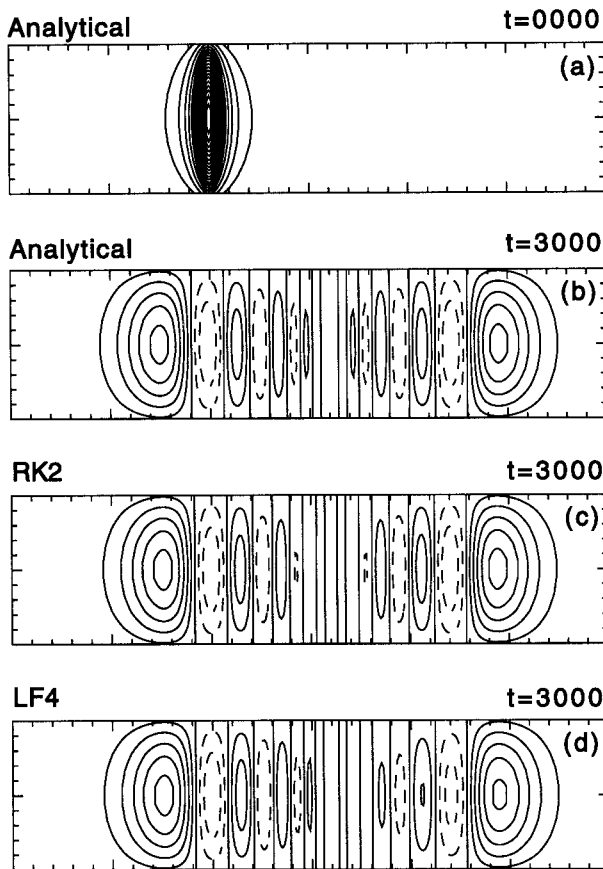


FIG. 3. (a) Perturbation  $\theta$  at  $t = 0$  for the nonhydrostatic gravity wave test, plotted with a contour interval of  $10^{-3}$  K. The plotted domain is 300 km by 10 km. (b) Analytical solution for perturbation  $\theta$  at  $t = 3000$  s, plotted with a contour interval of  $0.5 \times 10^{-3}$  K, for the analytic solution. (c) Perturbation  $\theta$  at  $t = 3000$  s for the RK2 model. (d) Same as (c), except for the leapfrog model.

term integrations may require a more stable treatment of the Coriolis terms. One possibility is a forward-backward integration of these terms on the small time step (Pielke 1984, 291). We have not encountered any sign of instability in our simulations using these methods in

our simple model or in our complete compressible full-physics models.

In these tests, no horizontal or vertical filtering is used in either model and the only numerical filter included in the RK2 scheme is a divergence damping filter (SK92), with a damping coefficient  $\alpha = 0.02$ . The leapfrog scheme uses spatially centered fourth-order horizontal and second-order vertical differencing for the advection terms. The same divergence damping filter is applied to the leapfrog scheme, and an Asselin time filter with a value of 0.1 is used to couple successive time levels together. Both models use a C grid staggering, and finite differencing of the divergence and pressure gradient terms are approximated to second order as in SK92. The small-time-step algorithms are identical in the leapfrog and RK2 models.

Figure 3 shows the results for a grid aspect ratio of  $\Delta x = \Delta z = 1$  km, the nonhydrostatic inertia-gravity wave case. The parameters used are identical to those used for the nonhydrostatic case in SK94 and are listed in Table 1. The initial condition and analytical solution at  $t = 3000$  s are shown in Figs. 3a and 3b, and Fig. 3c shows the  $\theta$  solution from the RK2 scheme at 3000 s. The RK2 scheme appears to closely reproduce the analytical solution shown in Fig. 3b. The  $\theta$  perturbations are symmetric about the center of the domain. In contrast, the solution from the leapfrog scheme (Fig. 3d) is not symmetric, with the  $\theta$  perturbations being somewhat reduced in the right half of the domain. Table 1 shows that for  $n_s = 6$ , the RK2 model is about 10% more expensive and  $\theta$  perturbation rms error is about 10% smaller than in the leapfrog model.

Figure 4 shows the results at 60 000 s from simulations using a grid aspect ratio of  $(\Delta x/\Delta z) = 20$ , the hydrostatic inertia-gravity wave case. The first experiments use a 200-s time step as in SK94, and the RK2 solution, shown in Fig. 4b again reproduces very closely the analytical solution shown in Fig. 4a as well as maintaining symmetric  $\theta$  perturbations about the center of the domain. The solution from the leapfrog scheme (Fig. 4c) is again not symmetric, with the  $\theta$  field having re-

TABLE 1. Efficiency and accuracy statistics for the leapfrog and RK2 time-split schemes for hydrostatic and nonhydrostatic inertia-gravity wave tests. Abbreviations LF and RK2 refer to the Runge-Kutta and leapfrog models described in the text.

	$\Delta t$ (s)	Mean $U\Delta t/\Delta x$	Time steps	No. of small steps	CPU time (s)			rms error (K)
					Nonacoustic	Acoustic	Total	
Nonhydrostatic inertia-gravity wave								
LF	12	0.24	250	6	1.75	8.37	10.12	$2.177 \times 10^{-3}$
RK2	12	0.24	250	6	4.84	6.27	11.11	$1.950 \times 10^{-3}$
Hydrostatic inertia-gravity wave								
LF	200	0.2	300	6	2.10	10.13	12.23	$2.952 \times 10^{-4}$
RK2	200	0.2	300	6	6.54	7.53	14.08	$2.796 \times 10^{-4}$
LF	200	0.2	300	12	2.10	20.15	22.25	$2.974 \times 10^{-4}$
RK2	200	0.2	300	12	6.54	15.17	21.72	$2.811 \times 10^{-4}$
LF	600	0.6	100	12	0.69	6.64	7.34	$3.174 \times 10^{-4}$
RK2	600	0.6	100	12	2.19	5.01	7.20	$2.050 \times 10^{-4}$

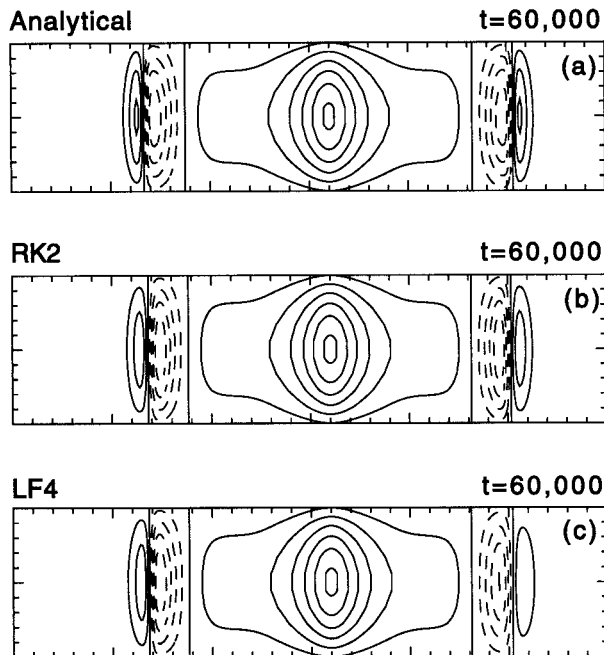


FIG. 4. (a) Perturbation  $\theta$  at  $t = 60\,000$  for the hydrostatic inertia-gravity wave test, plotted with a contour interval of  $0.5 \times 10^{-3}$  K. The plotted domain is  $6000$  km by  $10$  km. (b) Perturbation  $\theta$  at  $t = 60\,000$  s for the RK2 model. (c) Same as (b) except for the leapfrog model.

duced perturbations in the right half of the domain. The rms solution errors are similar in the cases that use the  $200$ -s time step and  $n_s = 6$ . Also shown in Table 1 are rms errors for the same simulation with time steps of  $200$  s with  $n_s = 12$  and  $600$  s with  $n_s = 12$ . The solution error in the RK2 scheme increases about the same as the leapfrog scheme when  $n_s$  increases. Interestingly, as the large time step increases, the rms error in the leapfrog scheme increases slightly, while the error in the RK2 solution is reduced by  $30\%$ . This is likely due to the fact that as the advective Courant number increases, the phase errors in the leapfrog scheme also increase. The total amount of dissipation in the RK2 scheme is proportional to the number of time steps taken, therefore the RK2 solution error decreases as the number of time steps is reduced from  $300$  to  $100$ .

#### b. Rising thermal simulations

Using the same codes as in the gravity wave simulations, the RK2 scheme's accuracy and stability is examined for a strongly nonlinear flow, the numerical simulation of a rising thermal in an adiabatic atmosphere. This problem is similar to the one presented by Carpenter et al. (1990), except that here a uniform horizontal flow of  $20 \text{ m s}^{-1}$  is introduced so that the thermal is transported laterally in a horizontally periodic domain. The grid spacing is  $125 \text{ m}$  in both the  $x$  and  $z$  directions, and the domain is  $20 \text{ km}$  wide and  $10 \text{ km}$

deep. The initial thermal has a radius of  $2 \text{ km}$  and is placed in the center of the domain at a height of  $2 \text{ km}$  with a potential temperature excess of  $2^\circ$ . A time step of  $2 \text{ s}$  is used and the mean horizontal Courant number is  $0.32$ . The solution is integrated for  $1000 \text{ s}$ , such that the rising thermal should be located in the center of the domain and the solution should remain symmetric. Figure 5 shows the solutions for the leapfrog and the RK2 schemes. Both thermals have risen nearly to the top of the domain (Figs. 5a,c). The RK2  $\theta$  field is nearly symmetric with some numerical oscillations located near the strong vertical gradients. The leapfrog  $\theta$  field is much less symmetric than the RK2 solution, and even more significant spurious oscillations are noted. Larger differences are seen in the vertical velocity fields (Figs. 5b,d). The leapfrog vertical velocity is clearly not symmetric, and there are numerical oscillations in the trailing wake behind the thermal. The RK2 vertical velocity field is nearly symmetric, with no oscillations present in the solution. These results indicate that the inherent damping and reduced phase errors associated with the RK2 scheme generate a more accurate solution than the fourth-order leapfrog solution, and the RK2 scheme has remained stable, even when the flow is strongly nonlinear.

All of these test problems indicate that the RK2 scheme performs as well, or even better than the fourth-order leapfrog scheme. As expected, the tests show that two evaluations of the advection terms in the RK2 scheme result in a considerably more costly advection algorithm than in the leapfrog formulation. However, the RK2 scheme requires only three-quarters the number of small time steps (per large time step) compared with the leapfrog scheme, thus the costs of the two schemes are comparable, especially when  $n_s > 10$ . Given the ability to easily incorporate limiters (monotonicity), the more selective dissipation in the RK2-based third-order upwind advection scheme compared with the filters used in leapfrog models, and the full second-order temporal accuracy of the advection operators, the RK2 scheme is computationally competitive with the leapfrog scheme.

#### 4. Discussion

We have presented a new forward-in-time splitting method for integrating the elastic equations. Using the RK2 scheme as the time integrator for the large time step, this method has been combined with the forward-backward scheme in a manner similar to the KW method such that the scheme produces fully second-order-accurate integration for advection and gravity wave propagation. The RK2 split scheme uses upwind discretizations for the advection derivatives and can be easily combined with standard vertically semi-implicit techniques so as to improve computational efficiency when the grid aspect ratio becomes large. A stability analysis of the RK2-based split scheme shows that it is stable

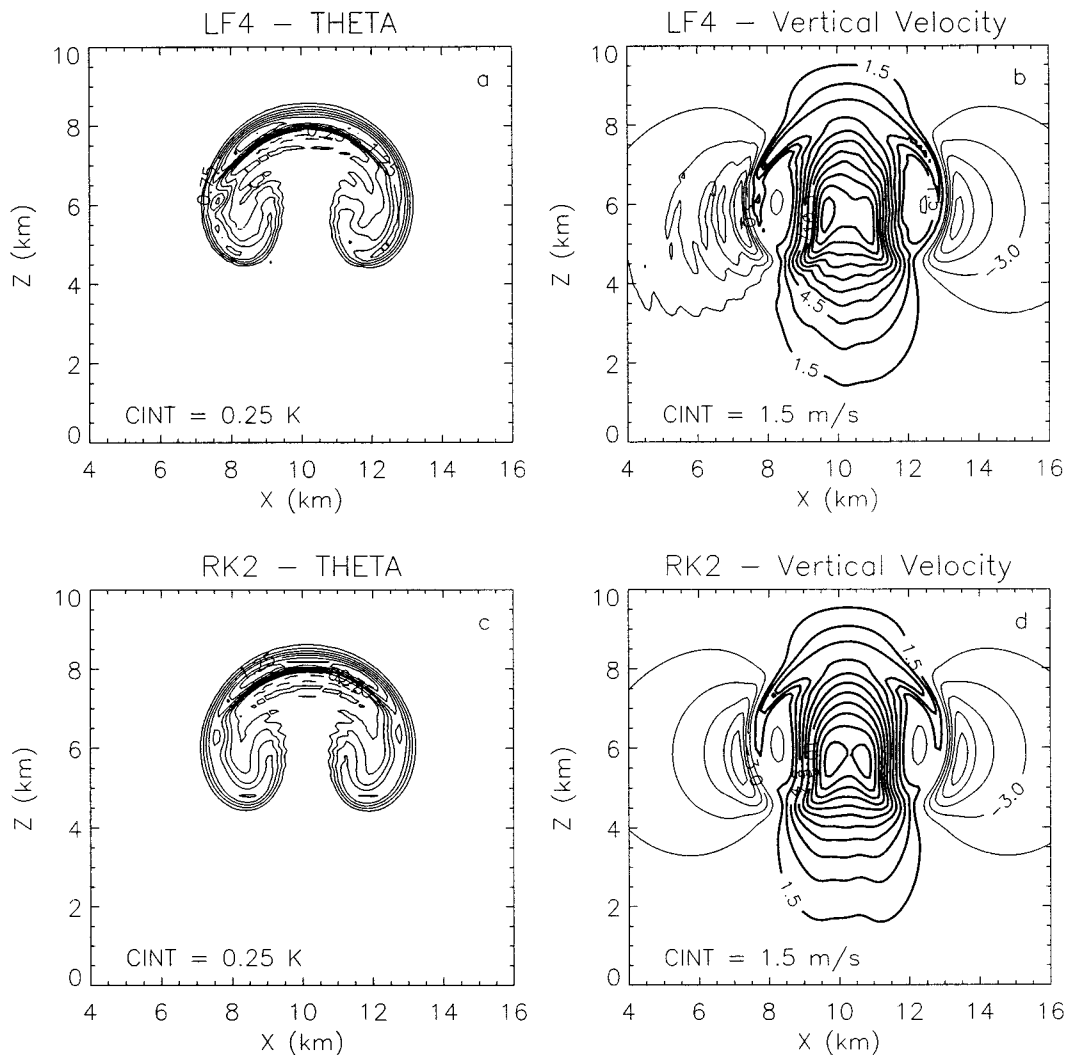


FIG. 5. (a) Perturbation  $\theta$  at  $t = 1000$  for the leapfrog solution to the rising thermal problem, plotted with a contour interval of 0.25 K. (b) Vertical velocity at  $t = 1000$  for the leapfrog solution to the rising thermal problem, plotted with a contour interval of 1.5  $\text{m s}^{-1}$ . Thick lines are positive contours, thin lines are negative contours. (c) Same as (a) except for the RK2 solution. (d) Same as (b) except for the RK2 solution.

for a wide range of advective and acoustic wave Courant numbers, and integrations reveal that the RK2 and KW leapfrog schemes generate similar solutions when the advective Courant number is small. As the time step and the advective Courant number increase, the RK2 scheme generates a somewhat more accurate solution than the KW leapfrog scheme.

The RK2 scheme is being used successfully in a full-physics nonhydrostatic model—the Collaborative Model for Multiscale Atmospheric Simulation [COMMAS, Wicker and Wilhelmson (1995)]. The implicit damping properties associated with the RK2's third-order horizontal differencing allows for a significant reduction in the value of horizontal fourth-order filtering applied to the momentum fields (typically by a factor of 20). As was the case for the leapfrog version of COMMAS, the RK2 scheme for momentum and pressure is combined

with a monotonic upwind-biased forward time scheme for the advection of scalar variables. The combination of the RK2 splitting scheme for the momentum and pressure equations with forward-in-time advection and mixing for the scalar equations has shown to be an accurate and robust methodology for a wide variety of simulations. We have found that the RK2 model requires about 10% more CPU time for the dynamics than the leapfrog model for a given computational grid and time step, while qualitatively the solutions appear to be better resolved than solutions obtained from the COMMAS leapfrog model.

Aspects of the full-physics model formulation using the RK2 scheme deserve further comment. In both the RK2 and leapfrog formulations, the turbulent mixing terms are handled forward-in-time (i.e., forward Euler). This is only first-order accurate in time, but this ap-

proach engenders only half the error of the leapfrog scheme for a given time step because the mixing is advanced from  $t$  to  $t + \Delta t$  in the RK2 model as opposed to  $t - \Delta t$  to  $t + \Delta t$  in the leapfrog model. Full second-order accuracy for the mixing terms can be obtained by integrating these terms using RK2 (like the advection terms), but this doubles the cost of the turbulence parameterizations because two evaluations of the mixing terms per time step are required. As noted in section 3, the Coriolis terms are differenced in a manner that is mildly unstable. The temporally first-order-accurate forward-in-time scheme can be replaced by the second-order-accurate RK2 scheme (at the cost of an additional Coriolis evaluation), resulting in a scheme that is less (although still) unstable. A stable treatment for the Coriolis terms using a forward-in-time scheme would require using a velocity estimate that is uncentered toward the  $t + \Delta t$  velocity; this would introduce damping and a return to first-order accuracy but would guarantee stability. As with the advection terms, the stability of any terms that possess purely imaginary frequencies require that their discrete counterpart possess complex frequencies with negative real parts (damping). Another solution would be to use a forward-backward scheme for the Coriolis terms (Pielke 1984, 291), which is conditionally stable for a large range of time steps and is a neutral scheme. This would require placing the computation of the Coriolis terms on the small time step.

Higher-order Runge-Kutta methods (such as the fourth-order Runge-Kutta method) could also be employed in a manner similar to the RK2 split scheme but would require additional evaluations of the large time step processes and additional small time steps. Estimates of the computational efficiency gained by using a higher-order Runge-Kutta scheme suggest that the increased cost in evaluating the advection is only marginally compensated by the increased time step allowed. Therefore we believe that the RK2 scheme is a good compromise between accuracy, efficiency, and complexity, given the

prevailing view that truncation errors associated with spatial discretizations are generally much larger than those associated with the temporal discretization in atmospheric models.

*Acknowledgments.* This work was partially funded under NSF Grant ATM-9318914. The authors also wish to thank Dr. Joseph Klemp of NCAR for many useful discussions on this topic.

#### REFERENCES

- Carpenter, R. L., Jr., K. K. Droegemeier, P. R. Woodward, and C. E. Hane, 1990: Application of the piecewise parabolic method (PPM) to meteorological modeling. *Mon. Wea. Rev.*, **118**, 586–612.
- Haltiner, G. J., and R. T. Williams, 1980: *Numerical Prediction and Dynamic Meteorology*. John Wiley and Sons, 447 pp.
- Hundsdoerfer, W., B. Koren, M. van Loon, and J. G. Verwer, 1995: A positive finite difference advection scheme. *J. Comput. Phys.*, **117**, 35–46.
- Klemp, J. B., and R. B. Wilhelmson, 1978: The simulation of three-dimensional convective storm dynamics. *J. Atmos. Sci.*, **35**, 1070–1096.
- Marchuk, G. I., 1974: *Numerical Methods in Weather Prediction*. Academic Press, 227 pp.
- Mesinger, F. M., 1977: Forward-backward scheme, and its use in a limited area model. *Contrib. Atmos. Phys.*, **50**, 200–210.
- Pielke, R. A., 1984: *Mesoscale Meteorological Modeling*. Academic Press, 612 pp.
- Press, W. H., B. F. Flannery, S. A. Teukolsky, and W. T. Vetterling, 1986: *Numerical Recipes*. Cambridge University Press, 818 pp.
- Skamarock, W. C., and J. B. Klemp, 1992: The stability of time-split numerical methods for the hydrostatic and nonhydrostatic elastic equations. *Mon. Wea. Rev.*, **120**, 2109–2127.
- , and —, 1994: Efficiency and accuracy of the Klemp-Wilhelmson time-splitting technique. *Mon. Wea. Rev.*, **122**, 2623–2630.
- Smolarkiewicz, P. K., 1984: A fully multidimensional positive definite advective transport algorithm with small implicit diffusion. *J. Comput. Phys.*, **54**, 325–362.
- Tremback, C. J., J. Powell, W. R. Cotton, and R. A. Pielke, 1987: The forward-in-time upstream advection scheme: Extension to higher orders. *Mon. Wea. Rev.*, **115**, 540–555.
- Wicker, L. J., and R. B. Wilhelmson, 1995: Simulation and analysis of tornado development and decay within a three-dimensional supercell thunderstorm. *J. Atmos. Sci.*, **52**, 2675–2703.